

Noise2Context: Context-assisted Learning 3D Thin-layer Low Dose CT Without Clean Data

Zhicheng Zhang, Xiaokun Liang, Wei Zhao*, and Lei Xing*

Abstract—Computed tomography (CT) has played a vital role in medical diagnosis, assessment, and therapy planning, *etc.* In clinical practice, concerns about the increase of X-ray radiation exposure attract more and more attention. To lower the X-ray radiation, low-dose CT is often used in certain scenarios, while it will induce the degradation of CT image quality. In this paper, we proposed a training method that trained denoising neural networks without any paired clean data. We trained the denoising neural network to map one noise LDCT image to its two adjacent LDCT images in a single 3D thin-layer low-dose CT scanning, simultaneously. In other words, with some latent assumptions, we proposed an unsupervised loss function with the integration of the similarity between adjacent CT slices in 3D thin-layer low-dose CT to train the denoising neural network in an unsupervised manner. For 3D thin-slice CT scanning, the proposed virtual supervised loss function was equivalent to a supervised loss function with paired noisy and clean samples when the noise in the different slices from a single scan was uncorrelated and zero-mean. Further experiments on Mayo LDCT dataset and a realistic pig head were carried out and demonstrated superior performance over existing unsupervised methods.

Index Terms—Low dose CT, Image denoising, Unsupervised learning, Deep learning

I. INTRODUCTION

COMPUTED tomography (CT) as a non-destructive imaging device for “inner vision” [1] has high hopes in clinical, industrial and other applications [2]–[5]. With the promotion of CT in clinical applications, however, the concern about the associated x-ray radiation dose which may potentially induce a public health issue has attracted wide public attention [6]. Therefore, the demand to optimize and reduce X-ray radiation dose becomes more imminent under the principle of ALARA (as low as reasonably achievable) [7]. Since the reduction of X-Ray dose will inevitably degrade the CT image quality, especially 3D thin-layer CT, how to obtain high-quality CT images with low-dose CT (LDCT) is a promising and practical research topic [6].

Generally, the low-flux acquisition by adjusting the X-ray tube current or exposure time to reduce single X-ray dose

in a single exposure [8]–[10] is common strategy. Since X-ray imaging is mainly a photon-noise dominated process with Poisson distribution [11], low X-ray exposure will lead to noisy projection, thus resulting in noisy CT images. To obtain high-quality LDCT images numerous LDCT reconstruction algorithms have been proposed in the past decades. All the methods can be mainly classified into three categories: sinogram filtration, iterative reconstruction, and post-processing. The key to sinogram filtration is the fact that the characteristics of noise in the sinogram domain are determined [12]. Bilateral filtering [13], [14], statistics-based nonlinear filters [15], and penalty of weighted least squares (PWLS) [16] were employed to lower the noise level of the noisy sinogram before CT image reconstruction, *e.g.* filtered back-projection (FBP). This kind of method is convenient and efficient while will give rise to spatial resolution loss or edge blurring [12].

The second category of LDCT reconstruction algorithms is the iterative reconstruction (IR). Benefiting from the boom in compressed sensing [17], [18], IR can reconstruct high-quality CT images from noisy sinograms directly by iteratively optimizing a special objective function. In this class of methods, CT scanning process [19]–[21] can be modeled with the integration of statistical properties of data in the projection domain as well as lots of prior information in the image domain. Specifically, total variation (TV) as the most well-known prior information was adopted to constrain the image gradient to be sparse [22], [23]. Also, nonlocal TV [24], low rank [25], dictionary learning [11], [26], *etc.* are also commonly used regularization terms. In addition to dictionary learning, IR do not require assistance from additional dataset, which is a data-independent type. Therefore, for each new LDCT reconstruction, IR needs to be re-optimized to obtain the best convergence point. Ignoring the demand of its related intensive computation, IR can greatly improve the reconstructed image quality. The last strategy for LDCT is image post-processing. To decrease the noise level of reconstructed CT images, nonlocal mean filtering (NLM) [27] and block matching (BM3D) [28] were utilized which are simple and efficient. With image post-processing, the image quality can be significantly improved, however, making the details over-smoothed due to the non-uniform noise in CT images.

With the rapid increase in amounts of data and soaring computing power, deep learning (DL) [29] has been employed in many application fields, such as computer vision [30], [31], autonomous driving [32], [33] and bio-medicine [34]–[36], *etc.* Recently, numerous DL-based methods have demonstrated their superiority of noise reduction on LDCT, which can be grouped into three categories. The first category is to use a

Manuscript received on May 05 2020, revised on XX XX 2020.

Z. Zhang, W. Zhao, X. Liang and L. Xing are with the Department of Radiation Oncology, Stanford University, Palo Alto, CA 94306, USA (e-mail: zzc623@stanford.edu, xiaokun.leung@gmail.com, {zhaow85, lei}@stanford.edu.)

This work was partially supported by NIH (1 R01CA227713), Varian Medical Systems, and a Faculty Research Award from Google Inc.

Copyright (c) 2020 IEEE. Personal use of this material is permitted. Permission from IEEE must be obtained for all other uses, including reprinting/republishing this material for advertising or promotional purposes, collecting new collected works for resale or redistribution to servers or lists, or reuse of any copyrighted component of this work in other works.

neural network to simulate the CT reconstruction process [37]. This kind of method requires a fully connected layer, leading to high memory requirements, which is limited to the problem of small size reconstruction. To get rid of the memory limitation and reconstruct high-quality CT images from sinogram directly, many neural network-assisted frameworks have been proposed with the integration of conventional iterative reconstruction [9], [38], [39], which can be treated as the second category. They only use small-scale CNN to simulate some simple components of the iterative algorithm, reduce the complexity of CNN, and improve the interpretability of the network. The third category is to use advanced DL techniques to optimize the architecture of the neural network to deal with CT images reconstructed by analytic algorithm [40]–[42]. Shan *et al.* proposed a modularized deep neural network and obtained competitive performance compared to commercial algorithms with the guide by domain experts in a task-specific fashion [35]. In addition, generative adversarial networks (GAN) [43], [44], residual learning [45]–[47] and reinforcement Learning [48], *etc* have also been employed for the network design.

The above mentioned DL-based LDCT reconstruction methods have obtained significant superiority over conventional analytic algorithms, which make deep CT reconstruction as a new frontier [49], however, their performance lies in amounts of the paired training dataset. The requirement of a high-quality paired training dataset often becomes the bottleneck of this kind of algorithms, since a large amount of training data is normally not available in some scenarios. Especially for the sinogram dataset which is harder to clinically obtain without cooperation from vendors. Therefore, training a high-performance LDCT reconstruction model with only noise CT images is a reasonable and realistic task.

Very recently, several preliminary explorations about unsupervised image denoising have been developed. In the natural image domain, Noise2noise (N2N) [50] makes full of the independence of noise in two scans with the assumption of zero-mean independent noise. To get rid of continuous multiple scans, Noise2Void (N2V) [50] predicts the artificially missing pixels from values of its neighbors. Noise2Sim [51] learns the mapping function between central pixels and their similar patches in the same noise images. All of these algorithms can obtain good performance on single image denoising while will ignore image context in 3D imaging.

In this work, we aim to reconstruct 3D thin-layer low-dose CT images that do not require any paired clean data. With some latent assumptions: (1) The noise embedded in the different layers of 3D FBP-reconstructed CT images is zero-mean and independent and (2) There is a strong similarity between adjacent CT slices in one patient, we can derive an unsupervised loss function based only on the similarity between adjacent CT slices. Based on the unsupervised loss function, the denoising network, *Noise2Context* (N2C), is then trained to map one noise realization to its two adjacent LDCT images, which can be seen in Fig. 1. Without ground truth as the supervision, the proposed N2C has two training strategies. (1) $N2C^M$: Train N2C on amounts of 3D patient LDCT scans offline and then apply the well-trained model to test new

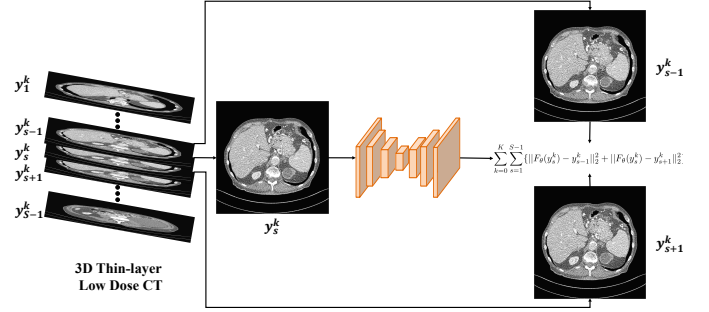


Fig. 1: The flowchart of the proposed method. For a 3D thin-layer LDCT. We can map each slice, y_s^k , to its two adjacent LDCT images, y_{s-1}^k and y_{s+1}^k , simultaneously.

patient cases. (2) $N2C^S$: Train and test N2C on the same 3D LDCT images to be reconstructed which can be in a patient-specific manner. The proposed method was evaluated on Low-dose CT Challenge dataset [52] for quarter-dose CT imaging and a realistic pig head with our in-house CBCT system. Experimental results demonstrated improved performance and robustness compare to other common denoising algorithms.

Our main contributions are summarized as follows.

- 1) With some latent assumptions, we proposed an unsupervised loss function with the integration of the similarity between adjacent CT slices in 3D thin-layer low-dose CT which can be employed as supervision to train corresponding deep neural networks.
- 2) With the proposed unsupervised loss function, we present an effective deep learning-based LDCT reconstruction algorithm which can be trained with different strategies to carry out the trade-off between performance and speed.
- 3) The performance and robustness of the proposed N2C have been demonstrated on the Mayo LDCT dataset and a realistic pig head with our in-house CBCT system.

The remainders of this paper are organized as follows. We elaborate our framework in Section II. The experiments and results are presented in Section III. We further discuss the key issues of our method in Section IV and draw the conclusions in Section V.

II. METHODOLOGY

A. Preliminary

For LDCT image denoising, the basic mathematical model can be formulated as: $y = x + n$, $y \in R^{M \times N}$ is the noisy LDCT image, $x \in R^{M \times N}$ is the clean CT image, NDCT, $n \in R^{M \times N}$ denotes the noise, where M and N denote the row and column, respectively. To obtain clean NDCT image from y , the obvious solution is to train a neural network F with parameters θ according to the l_2 loss as Eq. (1):

$$\mathcal{L}_{\theta} = \sum_{i=0}^I \|F_{\theta}(y_i) - x_i\|_2^2 \quad (1)$$

To obtain a high-performance denoising neural network F according to Eq. (1), numerous high-quality paired LDCT

images and their NDCT counterparts are necessary, which provide the powerful driving force to supervised learning. However, data acquisition is nontrivial to obtain, which limits the application scenario of neural network-based methods regarding the LDCT denoising task clinically. In this work, without clean NDCT images as supervision, we focus on 3D thin-layer LDCT in an unsupervised manner by making full of the similarity between adjacent 3D LDCT slices. With some reasonable assumptions, we can convert the unsupervised loss function to a supervised loss and efficiently train a high-performance denoising network without clean NDCT images as ground truth.

B. Noise2Context

To introduce N2C, some notations should be determined first. y_s^k , y_{s-1}^k , and y_{s+1}^k are three adjacent LDCT images of the k^{th} patient, x_s^k , x_{s-1}^k , and x_{s+1}^k are their clean counterparts, n_s^k , n_{s-1}^k , and n_{s+1}^k are corresponding noise, s is the index of LDCT image. We can formulate the N2C as following Eq. (2) with l_2 loss.

$$\theta = \arg \min_{\theta} \sum_{k=0}^K \sum_{s=1}^{S-1} \{ \|F_{\theta}(y_s^k) - y_{s-1}^k\|_2^2 + \|F_{\theta}(y_s^k) - y_{s+1}^k\|_2^2 \} \quad (2)$$

Where θ demonstrates the network parameters. By introducing auxiliary variables, x_s^k , the Eq. (2) can be inferred to Eq. (3).

$$\begin{aligned} \theta = \arg \min_{\theta} \sum_{k=0}^K \sum_{s=1}^{S-1} \{ & 2\|F_{\theta}(y_s^k) - x_s^k\|_2^2 \\ & + 2(2x_s^k - y_{s-1}^k - y_{s+1}^k)^T F_{\theta}(y_s^k) \\ & - 2(2x_s^k - y_{s-1}^k - y_{s+1}^k)^T x_s^k \\ & + \|x_s^k - y_{s-1}^k\|_2^2 + \|x_s^k - y_{s+1}^k\|_2^2 \} \end{aligned} \quad (3)$$

From Eq. (3), we can see that the first term is the supervised l_2 loss. The last three terms are irrelevant to the network parameters θ . Since $y_s^k = x_s^k + n_s^k$, Eq. (3) can be rewritten as Eq. (4):

$$\begin{aligned} \theta = \arg \min_{\theta} \sum_{k=0}^K \sum_{s=1}^{S-1} \{ & 2\|F_{\theta}(y_s^k) - x_s^k\|_2^2 \\ & + \sum_{k=0}^K \sum_{s=1}^{S-1} \{ 2(2x_s^k - x_{s-1}^k - x_{s+1}^k)^T F_{\theta}(y_s^k) \} \\ & - \sum_{k=0}^K \sum_{s=1}^{S-1} 2(n_{s-1}^k)^T F_{\theta}(y_s^k) - \sum_{k=0}^K \sum_{s=1}^{S-1} 2(n_{s+1}^k)^T F_{\theta}(y_s^k) \} \end{aligned} \quad (4)$$

Inside the real human body, there is a strong similarity between adjacent CT slices in 3D thin-layer low-dose CT as long as thickness and spacing are small enough. So $2x_s^k$ can be closed to $x_{s-1}^k + x_{s+1}^k$, thus the second term in Eq. (4) is about 0 as long as $F_{\theta}(y_s^k)$ is bounded. For the last two terms, according to Lindeberg-Levy central limit theorem, they will converge to $E(2(n_{s-1}^k)^T F_{\theta}(y_s^k))$ and $E(2(n_{s+1}^k)^T F_{\theta}(y_s^k))$, respectively, when the number of LDCT images for network training $K \times (S - 1) \rightarrow \infty$.

For the last two terms, they are similar and we use the last term as example, which can be rewritten as conditional expectation in Eq. (5).

$$E((n_{s+1}^k)^T F_{\theta}(y_s^k)) = E(E^T(n_{s+1}^k | F_{\theta}(y_s^k)) F_{\theta}(y_s^k)) \quad (5)$$

Because of the randomness of the noise, a reasonable assumption is that $E(n_{s+1}^k | F_{\theta}(y_s^k)) \rightarrow 0$ [53].

As a consequence, we can obtain Eq. (6). From Eq. (6), we can see that if we use the adjacent two slices as the supervision. Under certain assumptions, the unsupervised problem is equivalent to having the ground truth as the supervision. In other words, for 3D thin-slice CT scanning, we can treat Eq. (2) as the loss function to train deep neural networks.

$$\begin{aligned} & \arg \min_{\theta} \sum_{k=0}^K \sum_{s=1}^{S-1} \{ \|F_{\theta}(y_s^k) - y_{s-1}^k\|_2^2 + \|F_{\theta}(y_s^k) - y_{s+1}^k\|_2^2 \} \\ = & \arg \min_{\theta} \sum_{k=0}^K \sum_{s=1}^{S-1} \{ 2\|F_{\theta}(y_s^k) - x_s^k\|_2^2 \} \end{aligned} \quad (6)$$

III. EXPERIMENTS

In this section, we introduce the dataset used to train and evaluate the networks and describe the experimental setup and implementation details. We present the performance of our proposed method in denoising CT images and compare it to recent other methods including unsupervised methods and supervised baseline.

A. Dataset and Evaluation

1) *Dataset*: In this work, we used a publicly released patient dataset for 2016 NIH-AAPM-Mayo Clinic Low-Dose CT Grand Challenge. In this dataset, normal-dose abdominal CT images, NDCT, of both 1mm and 3mm slice thickness were taken from 10 anonymous patients and the corresponding quarter-dose CT images, LDCT, were simulated by inserting Poisson noise into the projection data. For unsupervised methods, theoretically, we can train and test them on the same LDCT images. To train a supervised DL-based model as a benchmark, we divided the original 10 training patient cases into 9/1 cases, related to the training/testing datasets, respectively. In total, we have 5410/526 2D CT images of 1mm slice thickness for training/quantitative testing.

2) *Evaluation*: Since we focus on how to obtain high-quality LDCT images in the real clinical setting, there are no any other NDCT images. In this work, we employ non-local mean (NLM) filter, total variation (TV) and Noise2void (N2V) [50] as contrast methods. For our method, it can be trained on the training dataset and then be tested on the testing dataset which we call N2C^M, or it can be trained and tested on the same testing dataset which we call N2C^S. To compare the performance of all the different methods, we carried out a visual inspection and quantitative metric evaluation such as root-mean-square-error (RMSE) and structure similarity index [54] (SSIM) for the generated CT images by all the methods.

For evaluation, we employed two different data sites. The first is the Mayo testing dataset including 1 patient case of 526 2D CT images of $1mm$ slice thickness due to the existed reference NDCT. To further test the generalizability and robustness in a real case, a pig head study was scanned using our in-house CBCT system at both the low/normal dose levels. After obtaining the 2D projection data, the analytic reconstruction algorithm, FDK, was used to reconstruct NDCT/LDCT images.

B. Implementation Details

The proposed framework was implemented in Python based on tensorflow [55] deep learning library. In the network training, all the images had a size of 512×512 . The Adam optimizer [56] was used to optimize the whole framework. The mini-batch size was set at 1 and the learning rate was set as $1e^{-4}$. The contrast methods, NLM and TV, can be found in the scikit-image library¹. We used the released version to implement N2V. In this work, to implement $N2C^S$, $N2C^M$, and the supervised model, we use standard U-net [57] with 32 basic feature-maps as the primary neural network, F , and Eq. (2) as the loss function. The supervised baseline is trained using Eq. (1) as the loss function.

C. Experimental Results on Mayo Testing Dataset

1) *Quantitative comparisons*: Fig. 2 shows the distribution of quantitative results (RMSE and SSIM) from all the 526 CT slices of the Mayo testing patient case - 'L506' which were processed by all the related methods. We can see that the supervised method provides a performance upper bound for all the unsupervised methods, which is consistent with [50], since there is a similar statistical distribution between the training dataset and the testing dataset and deep neural network can benefit from amounts of training datasets.

Compared to LDCT, all the unsupervised methods (NLM, TV, N2N, $N2C^S$, and $N2C^M$) can lower the RMSE and improve the SSIM. The performance improvement of N2N is limited. The RMSE and SSIM median values of all 526 CT images from $N2C^S$ and $N2C^M$ are superior to those from NLM, TV, and N2N. By observing the probability statistical density curve in Fig. 2, we can see that the quantitative results of 526 images from $N2C^M$ are more concentrated than that from $N2C^S$, even though their RMSE and SSIM median values are pretty close.

2) *Qualitative analysis*: For visual inspection, we extract 2 CT slices from patient, L506, to demonstrate the performance of the proposed method. The first is the abdominal CT image and the other is pelvic CT image. From Fig. 3, we can see that all the related methods can reduce the noise level of LDCT images. The supervised method provides the best performance, even its noise level is lower visually than the NDCT in Fig. 3 (A) and (A1). The potential reason is supervised methods can extract common features from amounts of training dataset to make up for deflection of the CT image. NLM will over-smooth

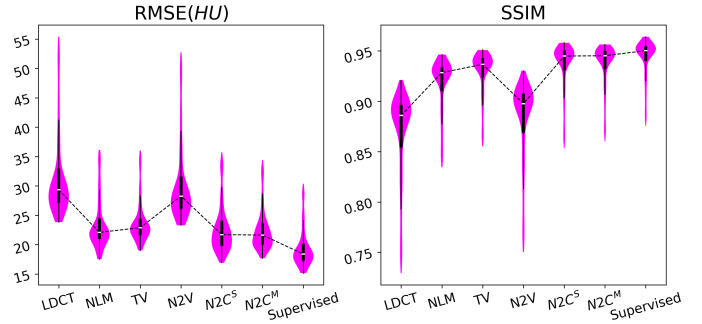


Fig. 2: The distribution of quantitative results for all the 526 CT images from patient 'L506'. In these violin plots, the white line shows the median value from each methods. Magenta shows the distribution of values.

the details both in (C) and (C1) and TV will induce the block effect in (D) and (D1), although NLM and TV can obtain good quantitative results seen in Fig. 2. In contrast, we can see that the CT images reconstructed by $N2C^M$ is closest to the reference NDCT image followed by $N2C^S$. This trend can be found in Fig. 5 by investigating how much details are left in the absolute difference images.

In the zoomed regions in Fig. 4 (marked by the red dotted rectangle in Fig. 3 (A)), we can see that both the low-contrast liver lesions (marked by the red dotted ellipses) and the blood vessels (marked by the yellow dotted ellipses) were clearly demarcated using $N2C^S$ and $N2C^M$ as opposed to the results of other methods. By the way, the quantitative results from this abdominal and pelvic case were shown directly below the corresponding results. Red and blue indicate the best and the second-best results, respectively. The supervised method gave the best performance in terms of RMSE and SSIM than others, which can be treated as the baseline for all the unsupervised methods. In all the unsupervised methods, the performance of $N2C^S$ and $N2C^M$ were superior to others. The RMSE of $N2C^M$ was lower than that from $N2C^S$ and the SSIM of $N2C^M$ was higher than that from $N2C^S$ in abdominal case but equal to that from $N2C^S$ in pelvic case. The possible explanation is that $N2C^M$ was trained with more training dataset than $N2C^S$, therefore, the feature extraction capability of the $N2C^M$ is stronger than $N2C^S$. All our visual observations are consistent with the quantitative terms as shown in Fig. 2.

D. Experimental Results on a Realistic Pig Head

To further validate the effectiveness of the proposed method, a realistic pig head was imaged using an in-house developed CBCT system with a flat-panel detector, the X-ray shape is a cone beam. The scanning protocol can be summarized as follows: X-ray tube voltage was set at 80 kV and then we obtained 3 LDCT scans when X-ray tube current were set at 2.2 mA for NDCT, 0.7 mA, 1.1 mA, and 1.6 mA for LDCT, respectively. In addition, the pixel size of X-ray detector 0.417 mm, source and detector distance 1510 mm, source and object distance 995 mm. 675 projections of size 1024×1024 over 360 degrees. After reconstruction by FDK, we can obtain 3D

¹<https://scikit-image.org/>

²<https://github.com/juglab/n2v>

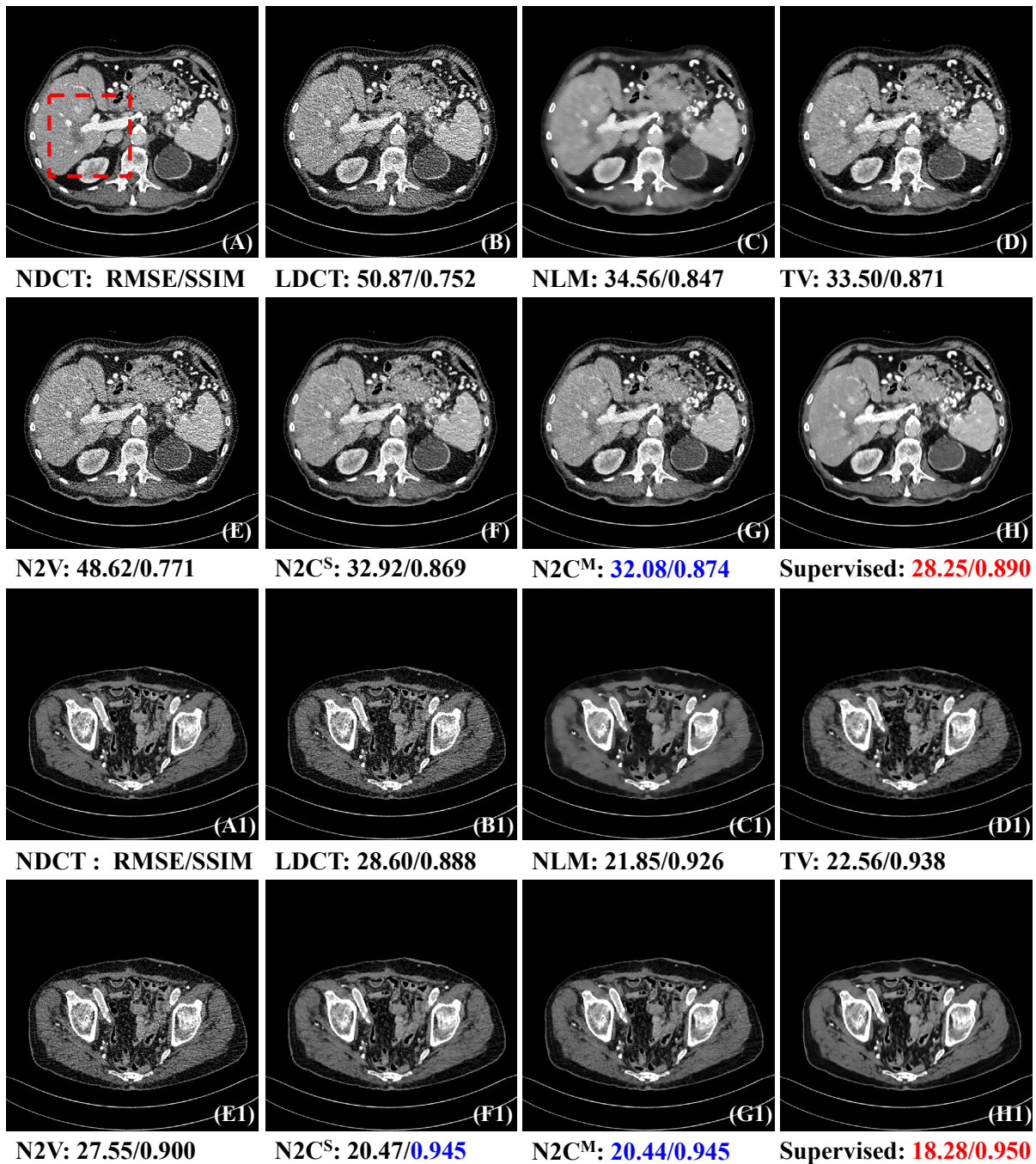


Fig. 3: Two visual comparisons from Mayo testing dataset including quantitative results. The display window is $[-100, 300]HU$. Red and blue indicate the best and the second-best results, respectively.

CBCT images with 200 CBCT images whose slice thickness is set at 0.5 mm , and then we can process these 200 CBCT images with all the related methods slice by slice.

Fig 6 shows the corresponding results from all the related methods when the X-ray tube current is set at 0.7 mA . The enlarged regions marked by the red dotted rectangle in NDCT (Fig 6 (A)) locate in the upper right corner of the corresponding images. It can be observed that all the methods eliminate noise to varying degrees, while N2C^S (Fig 6 (F)) gives the best performance. TV introduce the block effect which also exists in Fig. 3 (D). The denoising effect of N2V

(Fig 6 (E)) was not obvious. Extra artifacts (marked by the red arrow in Fig 6 (C) and the red ellipse in Fig 6 (H)) reduce the quality of the images. The above observation can be supported by the absolute difference images associated with different methods (Fig. 6 (B1-H1)). N2C^M has changed tiny structures marked by the orange arrows in Fig. 6 (G1) There is less detail left in Fig. 6 (F1). All the visual observations were consistent with the quantitative terms (RMSE and SSIM) as shown in Fig. 6 located below the corresponding CBCT images. Red and blue indicate the best and the second-best results, respectively.

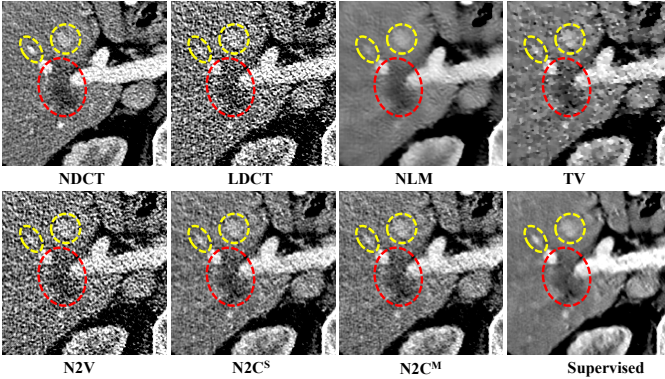


Fig. 4: The zoomed regions marked by the red box in Fig. 3 (A). The display window is $[0, 200]HU$

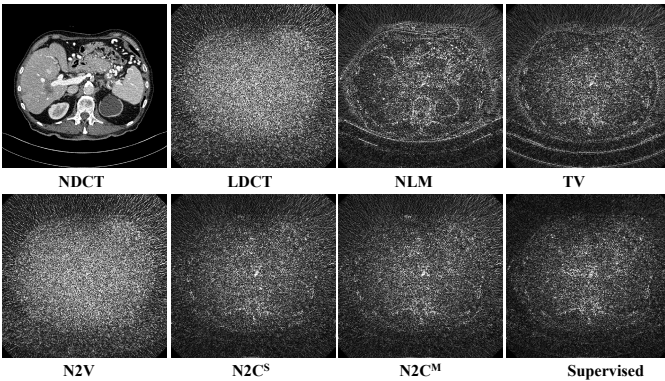


Fig. 5: The absolute difference maps from all the related methods. The display window is $[0, 100]HU$

E. Robustness

For deep neural networks, the performance is highly susceptible to the noise level of input. To evaluate the robustness of the proposed methods, we carry out all the experiments on different CBCT scans with different X-ray tube current ($0.7 mA$, $1.1 mA$, $1.6 mA$). Table I shows the quantitative results (MEAN \pm SDs) associated with different methods on the 3D realistic pig head at different noise levels, obtained by averaging the corresponding values of 200 images within a CBCT scan. Red and blue indicated the best and the second-best results, respectively. The proposed method, $N2C^S$ outperformed all the other methods in all the metrics significantly at all noise levels. The performance of deep neural network based methods ($N2C^M$ and Supervised baseline) which was pretrained on the training dataset decreases with the increase of noise level. This solid evidence is in strong agreement with our visual observations and demonstrates the robustness of the proposed method.

IV. DISCUSSION

X-ray radiation is a long-standing problem in clinical CT imaging. To reduce the X-ray radiation risk, lowering the X-ray tube current is a common method while will induce the degradation of CT image quality. To obtain a high-quality CT image at low-dose X-ray radiation, in this work, we aim to train a neural network to improve the quality of CT

images which were reconstructed by analytic reconstruction algorithms. To get rid of the reliance on amounts of the training dataset, with some latent assumptions, we can prove that the optimization of Eq. (2) is equivalent to the optimization of a supervised loss function with paired noisy and clean samples. For 3D CT patient-specific scanning, as long as the layer spacing is small, we can train the neural network in an unsupervised fashion according to the above conclusion. In this way, we could better utilize the context between different slice CT images of a single patient and obtain a robust low-dose CT reconstruction algorithm, alleviating the risk of X-ray radiation exposure to the patient.

Compared to conventional denoising methods, such as NLM and TV, the proposed method is a deep learning-based method and can extract common features from 3D images context, which get rid of the trouble of manually designed image prior, and thus eliminating some extra artifacts brought by manually designed image prior, such as block effect in Fig. 3 (D) and Fig. 6 (D). Compared to the supervised method, the proposed method has its superiority. The proposed method can be treated as a patient-specific method, which can be trained and tested on the same low dose CT images to be reconstructed. This manner can expand the applicability and practicability of the proposed method. In the experiment on realistic pig head, we can see that the performance of the supervised methods which was well-trained on the Mayo dataset suffers from significant performance degradation as the noise of the input image increases, because the weights of the supervised neural network are fixed and cannot be changed adaptively. However, our method can be fine-tuned or retrained with the low dose CT images to be reconstructed. Table I demonstrates the validity and superiority of the proposed method.

The success of the proposed approach rests on two assumptions on the property of noise and similarity between adjacent CT slices. The first one is that the noise was only required to be zero-mean and independent. The dependency can be achieved by 3D CT scanning, since different LDCT slices are reconstructed from different sinograms and zero-mean can be guaranteed with appropriate reconstruction algorithms [53]. The second is that we need a smaller thickness and spacing to ensure the strong similarity between adjacent CT slices. For different thickness and spacing, we can well train the proposed $N2C^S$ and compare the performance of our method horizontally with that of other methods, like what we have done in the experiment in this paper (see Fig. 2, Fig. 3, Fig. 4, Fig. 5, Fig. 6, and Table I). However, different thicknesses and spacing may cause inconsistencies in the low dose CT images to be tested. In other words, we cannot compare the effect of different thicknesses and spacing on the proposed method on the same dataset vertically. Therefore, we limit the application scenario of the proposed algorithm to 3D thin-slice CT scanning, and it can even be extended to other thin-layer imaging fields, such as MRI, PET, and Ultrasound, *etc.*

Although the advantages of the proposed method, there are still some limitations to this study. Since the input of the proposed method is the FBP-reconstructed CT images or FDK-reconstructed CBCT images, the input image itself weakens a lot of detail due to the low X-ray radiation. We do not expect

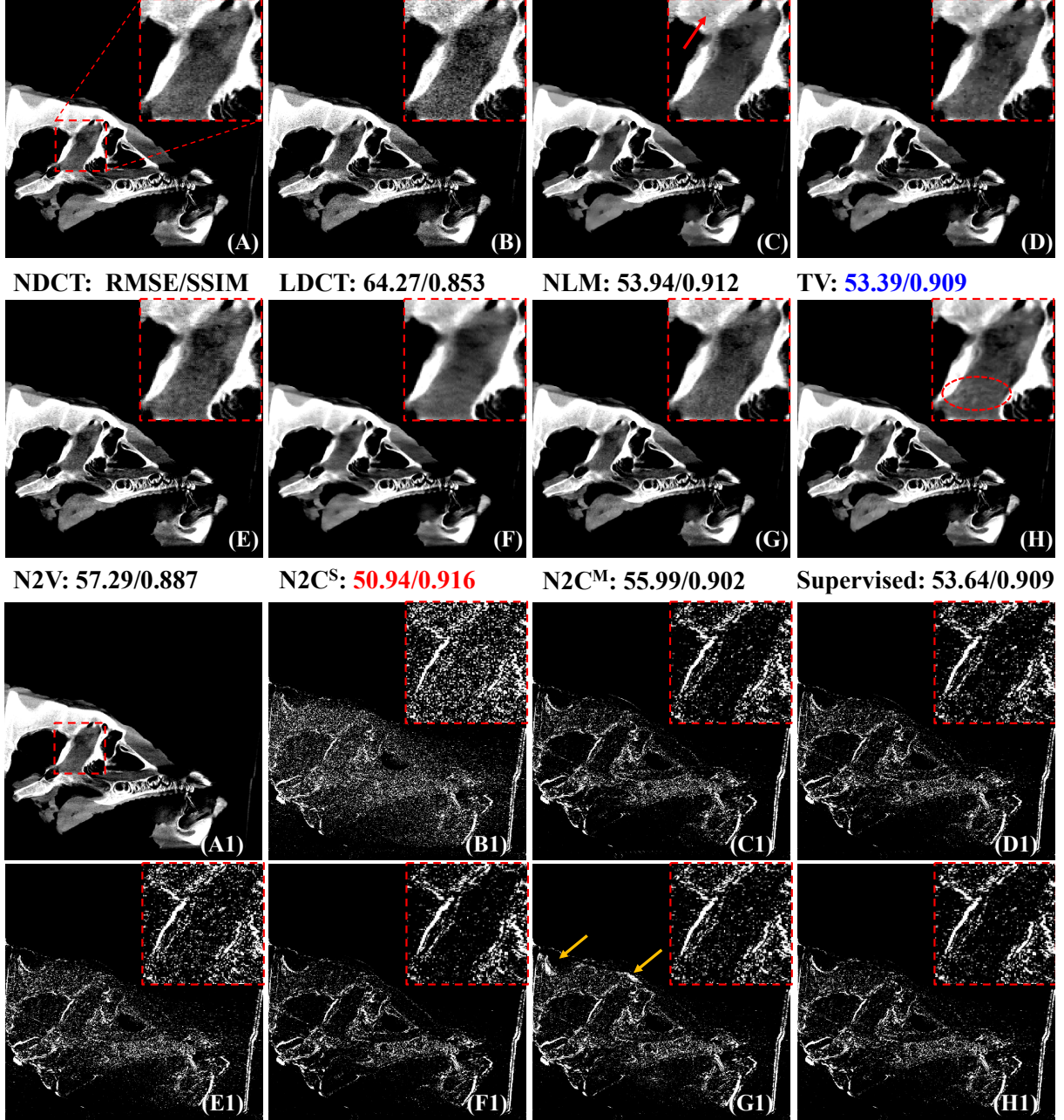


Fig. 6: The visual comparisons from the realistic pig head when the X-ray tube current is $0.7mA$. (A, A1): NDCT. (B, B1): LDCT. (C, C1): NLM. (D, D1): TV. (E, E1): N2V. (F, F1): N2C^S. (G, G1): N2C^M. (H, H1): Supervised. The display window in (A-H, A1) is $[-500, 200]HU$. The display window in the absolute difference images (B1-H1) is $[80, 160]HU$. Red and blue indicate the best and the second-best results, respectively.

TABLE I: Quantitative results (MEAN \pm SDs) associated with different methods on the 3D realistic pig head at different noise level. Red and blue indicate the best and the second-best results, respectively.

X-ray Tube Current		LDCT	NLM	TV	N2V	N2C ^S	N2C ^M	Supervised
$0.7mA$	RMSE(HU)	59.12 \pm 6.56	47.77 \pm 7.83	47.34 \pm 7.38	50.94 \pm 7.52	45.18 \pm 6.92	48.97 \pm 7.74	47.01 \pm 7.73
	SSIM	0.857 \pm 0.014	0.921 \pm 0.013	0.919 \pm 0.013	0.899 \pm 0.018	0.924 \pm 0.011	0.911 \pm 0.012	0.919 \pm 0.012
$1.1mA$	RMSE(HU)	53.12 \pm 6.77	45.23 \pm 8.12	44.78 \pm 7.76	47.70 \pm 7.82	44.12 \pm 7.59	46.34 \pm 7.97	45.01 \pm 8.19
	SSIM	0.883 \pm 0.011	0.928 \pm 0.010	0.927 \pm 0.010	0.912 \pm 0.013	0.929 \pm 0.009	0.922 \pm 0.010	0.927 \pm 0.010
$1.6mA$	RMSE(HU)	47.08 \pm 5.71	41.78 \pm 6.57	40.47 \pm 6.33	43.05 \pm 6.49	39.86 \pm 6.06	42.14 \pm 6.89	41.18 \pm 6.60
	SSIM	0.902 \pm 0.009	0.932 \pm 0.009	0.933 \pm 0.009	0.923 \pm 0.011	0.934 \pm 0.008	0.929 \pm 0.009	0.933 \pm 0.009

to generate strong outputs from weak inputs. Therefore, the supervised methods would be a performance upper bound for all the paired training data-independent methods. In Fig. 3, we can see that the performance of the supervised method is superior to the proposed method. Besides, we can obtain good performance with the pretrained $N2C^M$ when the training data and testing data have very similar data distribution (see the experiment on the Mayo dataset, Fig. 3). while there is a domain gap between the training data and testing data, we should use the testing dataset to retrain $N2C^S$, see the experiment on the realistic pig head. Therefore, we cannot guarantee the real-time performance of the proposed method.

V. CONCLUSION

In this work, we present a generalizable low dose CT image denoising method by address the optimization of Equ. (2) with some latent assumptions, which can be trained and tested on the same low dose CT images to be reconstructed in an unsupervised fashion. Our method not only gets rid of the complex artificial image priors but also amounts of paired high-quality training datasets. Various experiments demonstrate the effectiveness of our method and show the strong potential of our method to reduce X-ray radiation.

REFERENCES

- [1] G. Wang, H. Yu, and B. De Man, "An outlook on x-ray ct research and development," *Medical physics*, vol. 35, no. 3, pp. 1051–1064, 2008.
- [2] L. De Chiffre, S. Carmignato, J.-P. Kruth, R. Schmitt, and A. Weckenmann, "Industrial applications of computed tomography," *CIRP annals*, vol. 63, no. 2, pp. 655–677, 2014.
- [3] W. C. Scarfe, A. G. Farman, P. Sukovic *et al.*, "Clinical applications of cone-beam computed tomography in dental practice," *Journal-Canadian Dental Association*, vol. 72, no. 1, p. 75, 2006.
- [4] E. Seeram, *Computed tomography: physical principles, clinical applications, and quality control*. Elsevier Health Sciences, 2015.
- [5] J. P. Mathews, Q. P. Campbell, H. Xu, and P. Halleck, "A review of the application of x-ray computed tomography to the study of coal," *Fuel*, vol. 209, pp. 10–24, 2017.
- [6] D. J. Brenner and E. J. Hall, "Computed tomography—an increasing source of radiation exposure," *New England Journal of Medicine*, vol. 357, no. 22, pp. 2277–2284, 2007.
- [7] T. L. Slovis, "The alara concept in pediatric ct: myth or reality?" *Radiology*, vol. 223, no. 1, pp. 5–6, 2002.
- [8] H. Chen, Y. Zhang, W. Zhang, P. Liao, K. Li, J. Zhou, and G. Wang, "Low-dose ct via convolutional neural network," *Biomedical optics express*, vol. 8, no. 2, pp. 679–694, 2017.
- [9] J. He, Y. Yang, Y. Wang, D. Zeng, Z. Bian, H. Zhang, J. Sun, Z. Xu, and J. Ma, "Optimizing a parameterized plug-and-play admm for iterative low-dose ct reconstruction," *IEEE transactions on medical imaging*, vol. 38, no. 2, pp. 371–382, 2018.
- [10] Z. Tian, X. Jia, K. Yuan, T. Pan, and S. B. Jiang, "Low-dose ct reconstruction via edge-preserving total variation regularization," *Physics in Medicine & Biology*, vol. 56, no. 18, p. 5949, 2011.
- [11] Q. Xu, H. Yu, X. Mou, L. Zhang, J. Hsieh, and G. Wang, "Low-dose x-ray ct reconstruction via dictionary learning," *IEEE transactions on medical imaging*, vol. 31, no. 9, pp. 1682–1697, 2012.
- [12] Y. Ma, B. Wei, P. Feng, P. He, X. Guo, and G. Wang, "Low-dose ct image denoising using a generative adversarial network with a hybrid loss function for noise learning," *IEEE Access*, vol. 8, pp. 67 519–67 529, 2020.
- [13] A. Manduca, L. Yu, J. D. Trzasko, N. Khaylova, J. M. Kofler, C. M. McCollough, and J. G. Fletcher, "Projection space denoising with bilateral filtering and ct noise modeling for dose reduction in ct," *Medical physics*, vol. 36, no. 11, pp. 4911–4919, 2009.
- [14] L. Yu, A. Manduca, J. D. Trzasko, N. Khaylova, J. M. Kofler, C. M. McCollough, and J. G. Fletcher, "Sinogram smoothing with bilateral filtering for low-dose ct," in *Medical Imaging 2008: Physics of Medical Imaging*, vol. 6913. International Society for Optics and Photonics, 2008, p. 691329.
- [15] J. Wang, H. Lu, T. Li, and Z. Liang, "Sinogram noise reduction for low-dose ct by statistics-based nonlinear filters," in *Medical Imaging 2005: Image Processing*, vol. 5747. International Society for Optics and Photonics, 2005, pp. 2058–2066.
- [16] P. J. La Riviere, "Penalized-likelihood sinogram smoothing for low-dose ct," *Medical physics*, vol. 32, no. 6Part1, pp. 1676–1683, 2005.
- [17] D. L. Donoho, "Compressed sensing," *IEEE Transactions on information theory*, vol. 52, no. 4, pp. 1289–1306, 2006.
- [18] E. J. Candès, J. Romberg, and T. Tao, "Robust uncertainty principles: Exact signal reconstruction from highly incomplete frequency information," *IEEE Transactions on information theory*, vol. 52, no. 2, pp. 489–509, 2006.
- [19] M. Katsura, I. Matsuda, M. Akahane, J. Sato, H. Akai, K. Yasaka, A. Kunimatsu, and K. Ohtomo, "Model-based iterative reconstruction technique for radiation dose reduction in chest ct: comparison with the adaptive statistical iterative reconstruction technique," *European radiology*, vol. 22, no. 8, pp. 1613–1623, 2012.
- [20] Y. Yamada, M. Jinzaki, Y. Tanami, E. Shiomi, H. Sugiura, T. Abe, and S. Kuribayashi, "Model-based iterative reconstruction technique for ultralow-dose computed tomography of the lung: a pilot study," *Investigative radiology*, vol. 47, no. 8, pp. 482–489, 2012.
- [21] D. Volders, A. Bols, M. Haspelslagh, and K. Coenegrachts, "Model-based iterative reconstruction and adaptive statistical iterative reconstruction techniques in abdominal ct: comparison of image quality in the detection of colorectal liver metastases," *Radiology*, vol. 269, no. 2, pp. 469–474, 2013.
- [22] E. Y. Sidky and X. Pan, "Image reconstruction in circular cone-beam computed tomography by constrained, total-variation minimization," *Physics in Medicine & Biology*, vol. 53, no. 17, p. 4777, 2008.
- [23] E. Y. Sidky, Y. Duchin, X. Pan, and C. Ullberg, "A constrained, total-variation minimization algorithm for low-intensity x-ray ct," *Medical physics*, vol. 38, no. S1, pp. S117–S125, 2011.
- [24] H. Kim, J. Chen, A. Wang, C. Chuang, M. Held, and J. Pouliot, "Non-local total-variation (nltv) minimization combined with reweighted l1-norm for compressed sensing ct reconstruction," *Physics in Medicine & Biology*, vol. 61, no. 18, p. 6878, 2016.
- [25] J.-F. Cai, X. Jia, H. Gao, S. B. Jiang, Z. Shen, and H. Zhao, "Cine cone beam ct reconstruction using low-rank matrix factorization: algorithm and a proof-of-principle study," *IEEE transactions on medical imaging*, vol. 33, no. 8, pp. 1581–1591, 2014.
- [26] Y. Chen, L. Shi, Q. Feng, J. Yang, H. Shu, L. Luo, J.-L. Coatrieux, and W. Chen, "Artifact suppressed dictionary learning for low-dose ct image processing," *IEEE transactions on medical imaging*, vol. 33, no. 12, pp. 2271–2292, 2014.
- [27] Z. Li, L. Yu, J. D. Trzasko, D. S. Lake, D. J. Blezek, J. G. Fletcher, C. H. McCollough, and A. Manduca, "Adaptive nonlocal means filtering based on local noise level for ct denoising," *Medical physics*, vol. 41, no. 1, p. 011908, 2014.
- [28] D. Kang, P. Slomka, R. Nakazato, J. Woo, D. S. Berman, C. C. J. Kuo, and D. Dey, "Image denoising of low-radiation dose coronary ct angiography by an adaptive block-matching 3d algorithm," in *SPIE Medical Imaging*, 2013.
- [29] Y. LeCun, Y. Bengio, and G. Hinton, "Deep learning," *nature*, vol. 521, no. 7553, pp. 436–444, 2015.
- [30] A. Karpathy, G. Toderici, S. Shetty, T. Leung, R. Sukthankar, and L. Fei-Fei, "Large-scale video classification with convolutional neural networks," in *Proceedings of the IEEE conference on Computer Vision and Pattern Recognition*, 2014, pp. 1725–1732.
- [31] S. Ren, K. He, R. Girshick, and J. Sun, "Faster r-cnn: Towards real-time object detection with region proposal networks," in *Advances in neural information processing systems*, 2015, pp. 91–99.
- [32] M. Zhang, Y. Zhang, L. Zhang, C. Liu, and S. Khurshid, "Deeproad: Gan-based metamorphic testing and input validation framework for autonomous driving systems," in *Proceedings of the 33rd ACM/IEEE International Conference on Automated Software Engineering*, 2018, pp. 132–142.
- [33] G. P. Meyer, A. Laddha, E. Kee, C. Vallespi-Gonzalez, and C. K. Wellington, "Lasernet: An efficient probabilistic 3d object detector for autonomous driving," in *Proceedings of the IEEE Conference on Computer Vision and Pattern Recognition*, 2019, pp. 12 677–12 686.
- [34] M. J. K. Xing L, Giger M L, *Artificial Intelligence in Medicine: Technical Basis and Clinical Applications*. Elsevier St. Louis MO in press, 2020.
- [35] H. Shan, A. Padole, F. Homayounieh, U. Kruger, R. D. Khera, C. Nitiwarankul, M. K. Kalra, and G. Wang, "Competitive performance of a modularized deep neural network compared to commercial algorithms

- for low-dose ct image reconstruction,” *Nature Machine Intelligence*, vol. 1, no. 6, pp. 269–276, 2019.
- [36] L. Zou, S. Yu, T. Meng, Z. Zhang, X. Liang, and Y. Xie, “A technical review of convolutional neural network-based mammographic breast cancer diagnosis,” *Computational and mathematical methods in medicine*, vol. 2019, 2019.
- [37] T. Würfl, F. C. Ghesu, V. Christlein, and A. Maier, “Deep learning computed tomography,” in *International conference on medical image computing and computer-assisted intervention*. Springer, 2016, pp. 432–440.
- [38] J. Adler and O. Öktem, “Learned primal-dual reconstruction,” *IEEE transactions on medical imaging*, vol. 37, no. 6, pp. 1322–1332, 2018.
- [39] H. Chen, Y. Zhang, Y. Chen, J. Zhang, W. Zhang, H. Sun, Y. Lv, P. Liao, J. Zhou, and G. Wang, “Learn: Learned experts’ assessment-based reconstruction network for sparse-data ct,” *IEEE transactions on medical imaging*, vol. 37, no. 6, pp. 1333–1347, 2018.
- [40] H. Chen, Y. Zhang, W. Zhang, P. Liao, K. Li, J. Zhou, and G. Wang, “Low-dose ct via convolutional neural network,” *Biomedical optics express*, vol. 8, no. 2, pp. 679–694, 2017.
- [41] H. Shan, Y. Zhang, Q. Yang, U. Kruger, M. K. Kalra, L. Sun, W. Cong, and G. Wang, “3d convolutional encoder-decoder network for low-dose ct via transfer learning from a 2d trained network,” *IEEE Transactions on Medical Imaging*, vol. 37, no. 6, p. 1522, 2018.
- [42] J. Liu, Y. Zhang, Q. Zhao, T. Lv, W. Wu, N. Cai, G. Quan, W. Yang, Y. Chen, L. Luo *et al.*, “Deep iterative reconstruction estimation (dire): approximate iterative reconstruction estimation for low dose ct imaging,” *Physics in Medicine & Biology*, vol. 64, no. 13, p. 135007, 2019.
- [43] J. M. Wolterink, T. Leiner, M. A. Viergever, and I. Išgum, “Generative adversarial networks for noise reduction in low-dose ct,” *IEEE transactions on medical imaging*, vol. 36, no. 12, pp. 2536–2545, 2017.
- [44] Q. Yang, P. Yan, Y. Zhang, H. Yu, Y. Shi, X. Mou, M. K. Kalra, Y. Zhang, L. Sun, and G. Wang, “Low-dose ct image denoising using a generative adversarial network with wasserstein distance and perceptual loss,” *IEEE transactions on medical imaging*, vol. 37, no. 6, pp. 1348–1357, 2018.
- [45] H. Chen, Y. Zhang, M. K. Kalra, F. Lin, Y. Chen, P. Liao, J. Zhou, and G. Wang, “Low-dose ct with a residual encoder-decoder convolutional neural network,” *IEEE transactions on medical imaging*, vol. 36, no. 12, pp. 2524–2535, 2017.
- [46] X. Yin, Q. Zhao, J. Liu, W. Yang, J. Yang, G. Quan, Y. Chen, H. Shu, L. Luo, and J.-L. Coatrieux, “Domain progressive 3d residual convolution network to improve low-dose ct imaging,” *IEEE transactions on medical imaging*, vol. 38, no. 12, pp. 2903–2913, 2019.
- [47] E. Kang, W. Chang, J. Yoo, and J. C. Ye, “Deep convolutional framelet denoising for low-dose ct via wavelet residual network,” *IEEE transactions on medical imaging*, vol. 37, no. 6, pp. 1358–1369, 2018.
- [48] C. Shen, Y. Gonzalez, L. Chen, S. B. Jiang, and X. Jia, “Intelligent parameter tuning in optimization-based iterative ct reconstruction via deep reinforcement learning,” *IEEE transactions on medical imaging*, vol. 37, no. 6, pp. 1430–1439, 2018.
- [49] G. Wang, J. C. Ye, K. Mueller, and J. A. Fessler, “Image reconstruction is a new frontier of machine learning,” *IEEE transactions on medical imaging*, vol. 37, no. 6, pp. 1289–1296, 2018.
- [50] A. Krull, T.-O. Buchholz, and F. Jug, “Noise2void-learning denoising from single noisy images,” in *Proceedings of the IEEE Conference on Computer Vision and Pattern Recognition*, 2019, pp. 2129–2137.
- [51] C. Niu and G. Wang, “Noise2sim—similarity-based self-learning for image denoising,” *arXiv preprint arXiv:2011.03384*, 2020.
- [52] C. H. McCollough, A. C. Bartley, R. E. Carter, B. Chen, T. A. Drees, P. Edwards, D. R. Holmes III, A. E. Huang, F. Khan, S. Leng *et al.*, “Low-dose ct for the detection and classification of metastatic liver lesions: Results of the 2016 low dose ct grand challenge,” *Medical physics*, vol. 44, no. 10, pp. e339–e352, 2017.
- [53] D. Wu, K. Gong, K. Kim, X. Li, and Q. Li, “Consensus neural network for medical imaging denoising with only noisy training samples,” in *International Conference on Medical Image Computing and Computer-Assisted Intervention*. Springer, 2019, pp. 741–749.
- [54] Z. Wang, A. C. Bovik, H. R. Sheikh, and E. P. Simoncelli, “Image quality assessment: from error visibility to structural similarity,” *IEEE transactions on image processing*, vol. 13, no. 4, pp. 600–612, 2004.
- [55] M. Abadi, P. Barham, J. Chen, Z. Chen, A. Davis, J. Dean, M. Devin, S. Ghemawat, G. Irving, M. Isard *et al.*, “Tensorflow: A system for large-scale machine learning,” in *12th {USENIX} symposium on operating systems design and implementation ({OSDI} 16)*, 2016, pp. 265–283.
- [56] D. P. Kingma and J. Ba, “Adam: A method for stochastic optimization,” *arXiv preprint arXiv:1412.6980*, 2014.
- [57] O. Ronneberger, P. Fischer, and T. Brox, “U-net: Convolutional networks for biomedical image segmentation,” in *International Conference on Medical image computing and computer-assisted intervention*. Springer, 2015, pp. 234–241.
- [58] Z. Zhang, X. Liang, X. Dong, Y. Xie, and G. Cao, “A sparse-view ct reconstruction method based on combination of densenet and convolution,” *IEEE transactions on medical imaging*, vol. 37, no. 6, pp. 1407–1417, 2018.
- [59] H. Zhang, D. Zeng, H. Zhang, J. Wang, Z. Liang, and J. Ma, “Applications of nonlocal means algorithm in low-dose x-ray ct image processing and reconstruction: A review,” *Medical physics*, vol. 44, no. 3, pp. 1168–1185, 2017.
- [60] S. Niu, Y. Gao, Z. Bian, J. Huang, W. Chen, G. Yu, Z. Liang, and J. Ma, “Sparse-view x-ray ct reconstruction via total generalized variation regularization,” *Physics in Medicine & Biology*, vol. 59, no. 12, p. 2997, 2014.
- [61] Y. Han and J. C. Ye, “Framing u-net via deep convolutional framelets: Application to sparse-view ct,” *IEEE transactions on medical imaging*, vol. 37, no. 6, pp. 1418–1429, 2018.
- [62] H. Lee, J. Lee, H. Kim, B. Cho, and S. Cho, “Deep-neural-network-based sinogram synthesis for sparse-view ct image reconstruction,” *IEEE Transactions on Radiation and Plasma Medical Sciences*, vol. 3, no. 2, pp. 109–119, 2018.
- [63] Z. Chen, X. Jin, L. Li, and G. Wang, “A limited-angle ct reconstruction method based on anisotropic tv minimization,” *Physics in Medicine & Biology*, vol. 58, no. 7, p. 2119, 2013.
- [64] X. Jin, L. Li, Z. Chen, L. Zhang, and Y. Xing, “Anisotropic total variation for limited-angle ct reconstruction,” in *IEEE Nuclear Science Symposium & Medical Imaging Conference*. IEEE, 2010, pp. 2232–2238.
- [65] E. Y. Sidky, C.-M. Kao, and X. Pan, “Accurate image reconstruction from few-views and limited-angle data in divergent-beam ct,” *Journal of X-ray Science and Technology*, vol. 14, no. 2, pp. 119–139, 2006.
- [66] L. Shen, W. Zhao, and L. Xing, “Patient-specific reconstruction of volumetric computed tomography images from a single projection view via deep learning,” *Nature biomedical engineering*, vol. 3, no. 11, pp. 880–888, 2019.
- [67] H. Zhang, L. Zhang, Y. Sun, and J. Zhang, “Projection domain denoising method based on dictionary learning for low-dose ct image reconstruction,” *Journal of X-ray science and technology*, vol. 23, no. 5, pp. 567–578, 2015.
- [68] D. Karimi and R. K. Ward, “Sinogram denoising via simultaneous sparse representation in learned dictionaries,” *Physics in Medicine & Biology*, vol. 61, no. 9, p. 3536, 2016.
- [69] C. Jiao, D. Wang, H. Lu, Z. Zhang, and J. Z. Liang, “Multiscale noise reduction on low-dose ct sinogram by stationary wavelet transform,” in *2008 IEEE Nuclear Science Symposium Conference Record*. IEEE, 2008, pp. 5339–5344.
- [70] Y. Wang, W.-L. Chao, D. Garg, B. Hariharan, M. Campbell, and K. Q. Weinberger, “Pseudo-lidar from visual depth estimation: Bridging the gap in 3d object detection for autonomous driving,” in *Proceedings of the IEEE Conference on Computer Vision and Pattern Recognition*, 2019, pp. 8445–8453.
- [71] B. Zhu, J. Z. Liu, S. F. Cauley, B. R. Rosen, and M. S. Rosen, “Image reconstruction by domain-transform manifold learning,” *Nature*, vol. 555, no. 7697, pp. 487–492, 2018.
- [72] J. Lehtinen, J. Munkberg, J. Hasselgren, S. Laine, T. Karras, M. Aittala, and T. Aila, “Noise2noise: Learning image restoration without clean data,” *arXiv preprint arXiv:1803.04189*, 2018.